Journal of Physics: Conference Series **2934** (2025) 012021 doi:10.1088/1742-6596/2934/1/012021

Indirect control of ^{13}C nuclear spin in nitrogen vacancy center in diamond

Kritsana Saego* **and Sorawis Sangtawesin**

School of Physics, Institute of Science, Suranaree University of Technology, Nakhon Ratchasima, 30000, Thailand.

*E-mail: kritsana98.sae@gmail.com

Abstract. The nitrogen vacancy (NV) center in diamond is one of the solid-state spin systems that can be manipulated as a qubit for quantum computing. However, scaling up the system to perform as a quantum register is challenging due to weak dipole interaction between two NV centers. On the other hand, ^{13}C nuclear spins that reside within the diamond lattice can be used as additional qubits for scaling up the system, as they have hyperfine interactions with the NV center electronic spin. In general, nuclear spins exhibit a longer coherence time compared to the electron spin due to the lower gyromagnetic ratio. Nevertheless, this weak interaction also makes it difficult to directly control the nuclear spin via RF transition. In this work, we demonstrated a scheme to control and observe the dynamics of nuclear spin with a hyperfine splitting of 6.5 MHz using an indirect pulse sequence that operated only the electron spin in absence of any RF signal. Our results reveal a nuclear spin free precession with a gyromagnetic ratio of 6.9 ± 0.1 kHz/Gauss. Furthermore, one can observe the nuclear spin phase accumulation in electronic spin $m_s = -1$ manifold and show the reduced contrast results from incomplete population transfer during the operation.

1.Introduction

The nitrogen-vacancy (NV) center in diamond is one of the solid-state spin systems applicable to quantum technologies [1, 2, 3], which arises from the substitution of two adjacent carbon atoms in the diamond lattice by a nitrogen and a vacancy. It can be controlled using microwave pulse techniques and read out via an optical signal in ambient conditions [4, 5]. Although the electrons in the NV center can be easily controlled due to its large value of gyromagnetic ratio, it has relatively short coherence time due to the large environmental couplings. To achieve longer coherence time, we can utilize the nuclear spins from nearby carbon atoms with strong hyperfine interactions [6]. However, the nuclear spin systems are typically difficult to control and require the use of RF signals [7]. Several studies have attempted to control hybrid systems by leveraging interactions and using microwave control of electron and nuclear spins together [8, 9, 10]. In this study, we demonstrated indirect control of nuclear spin without applying RF signals and showed free precession of the nuclear spin and hyperfine effects. Additionally, we point out the effects of imperfect polarization so that the protocols may be improved in the future to mitigate these effects.

2. Experiment details

2.1 Sample

We used single-crystal electronic (ELSC) grade diamond with a low NV concentration (less than 0.03 ppb) purchased from Element Six Ltd. The diamond plate size is 2 x 2 mm^2 with a thickness of 0.5 mm. The sample was implanted with ^{15}N with an energy of 30 keV and annealed to form NV centers [11]. The sample is attached to the PCB board fabricated with a coplanar waveguide design, which has a characteristic impedance close to 50 ohms. A 25 μm aluminum wire was stretched above the sample for carrying the microwave signal to the sample (see figure 1(a)). Magnetic field $\boldsymbol{B}$ was applied to the sample with a permanent magnet that can be adjusted to tune the magnetic field orientation along one of the NV center axes.

2.2 Confocal microscope

The photoluminescence from NV center was collected by using a home-built confocal microscope show in figure 1(a). The excitation source is a green laser with a wavelength of 532 nm (Coherent OBIS 532) that was aligned to the sample by following the green path shown in figure 1(a). We used an acousto-optic modulator (G&H AOMO 3080-120) as a control shutter for the green laser, then coupled the laser beam with the single-mode fiber coupler (Thorlabs PAF2-A7A). A galvo mirror (Thorlabs GVS 212/M) scans the laser on the sample in two directions (x-y plane) via a 4f-relay lens with a focal length of 150 mm (Edmund Optics 49-390). The beam was focused onto the sample with a 100x objective with an NA of 0.9 and a working distance of 1 mm (Olympus MPLFLN100X). We installed the sample on the piezo stage to make this system capable of fine focusing a confocal plane. After the NV centers are excited, they emit photons with a spectrum from 600 – 800 nm, which are then collected by the same focusing objective. The photons follow the same but reversed path as the green to the dichroic mirror (Thorlabs DMLP567), where the fluorescence photons are separated and focused into a fiber-coupled avalanche photodiode detector (APD). We placed a 600-nm long-pass filter (Thorlabs FELH600) in front of the APD to prevent the excitation beam from entering the detector. The detector then emits signals in terms of pulses according to each photon detected. The NV center image taken by our setup is shown in figure 1(c). We selected the NV center in the area close to aluminum wire to achieve large field amplitudes of the AC magnetic field signal from the microwave sources.

2.3 Microwave instrument

The microwave setup for our experiment is shown in figure 1(b). We used two sources of the microwave generator (RIGOL DSG836A and ROHDE&SCHWARZ SMBV100B). The generated signals are controlled by a microwave switch (ZASWA-2-50DRA+). We used a pulse generator (SpinCore Technologies Pulse Blaster ESR-PRO500) connected to a transistor-transistor logic (TTL) channel to control the timing trigger of the microwave signal and green laser. Before the signals go to an amplifier (ZHL-15W-422-5+), we use two filters, a high-pass filter (VHF-1600+) and a low-pass filter (LF-3000+) after the two microwave switches to eliminate higher and lower frequency harmonics from switching. In addition, we used two sets of –3 dBm attenuator (VAT-3+) and –10 dBm attenuator (VAT-10+) to prevent the signal from exceeding the +7dBm limitation of the amplifier, then combine the signals from each sources by using an RF combiner (ZFRSC-42-S+). After amplification, the combine signal is directed through the circulator (DITOM D3C2040) to protect the reflected signal from the sample from going back to the amplifier. The reflected signal from the last port of the circulator is blocked by a 50 Ω terminator (MCL BW-530W20+ and ANNE-50+). Finally, before passing the signal to the sample, we used a high-pass filter (VHF-

1600+) to filter out the additional amplifier noise, and after the sample we attenuate and monitor the signal via an oscilloscope.

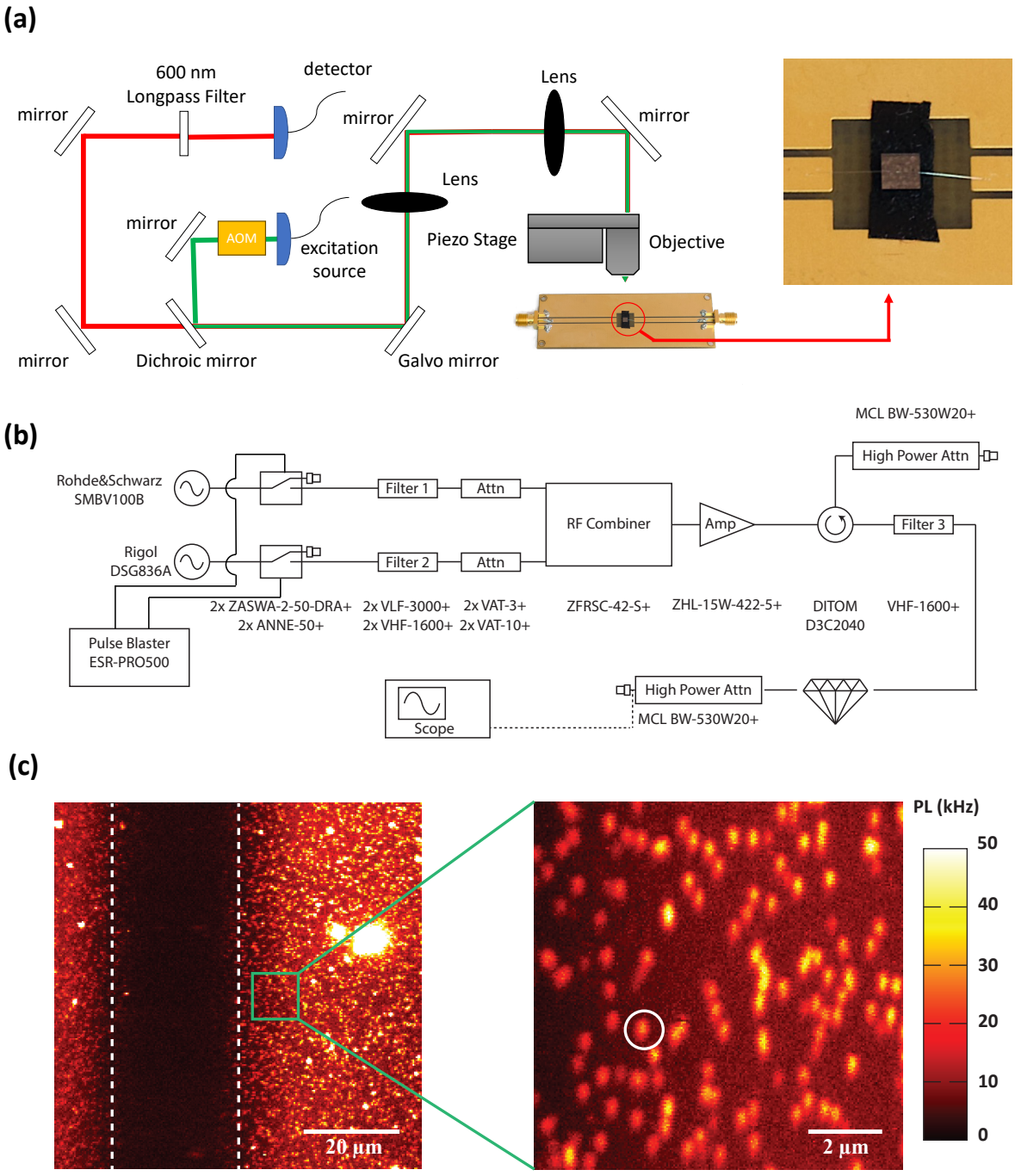

Figure 1. (a) The schematic for the confocal microscope setup. The NV sample is attached to the PCB board based on the coplanar waveguide design, and a 25 µm aluminum wire above the sample is used to carry the microwave signal to the sample. (b) The microwave setup diagram. (c) The picture of the diamond surface that was taken by the confocal microscope with the scanning area 80 x 80 µm^2 (left) and 10 x 10 µm^2 (right); the dash line is the aluminum wire observed under the confocal microscope. White circle indicates the NV center used in this experiment.

3. Results and discussion

3.1 System characterization

The electronic ground state of the NV center is a spin triplet system, consisting of a spin quantum number $m_s = 0$ and $m_s = \pm 1$, where the state $m_s = \pm 1$ are degenerate at zero magnetic field. We can distinguish the spin states by applying an external magnetic field that causes the Zeeman splitting [12]. The electron spin state can be determined from the measurement of the NV fluorescence intensity [13]. Surrounding the NV center are the carbon atoms which are 98.9% spinless ^{12}C, and 1.1% of spin-½ ^{13}C, consisting of spin up $|\uparrow\rangle$ and spin down $|\downarrow\rangle$ states. Each ^{13}C has a hyperfine interaction with the NV center electron spin, which gradually reduces as they are located farther away from the NV center [14]. We can use this interaction to control the nuclear spin, with the dynamics of the system described by the Hamiltonian

$$\hat{H}/h = D\hat{S}_z^2 + \gamma_e \boldsymbol{B} \cdot \hat{\boldsymbol{S}} + \gamma_c \boldsymbol{B} \cdot \hat{\boldsymbol{I}} + \hat{\boldsymbol{S}} \cdot \boldsymbol{A} \cdot \hat{\boldsymbol{I}}. \quad (1)$$

Where $\hat{\boldsymbol{S}} = (\hat{S}_x, \hat{S}_y, \hat{S}_z)$ and $\hat{\boldsymbol{I}} = (\hat{I}_x, \hat{I}_y, \hat{I}_z)$ are the electron spin and nuclear spin operators. $D = 2.87$ GHz is the zero-field splitting along the NV axis. The gyromagnetic ratio of the electron is $\gamma_e =$ 2.8 MHz/G, and $\boldsymbol{B}$ is the magnitude of the external magnetic field. The gyromagnetic ratio of the ^{13}C nuclear spin is $\gamma_c = 1.07$ kHz/G, and $\boldsymbol{A}$ is hyperfine tensor of the ^{13}C, which is different for each ^{13}C in different lattice locations.

By addressing an appropriate ^{13}C with strong coupling, we can access and control the nuclear spin by only applying the microwave to the electron spin. The general energy diagram of a single ^{13}C couple to an electron spin in the NV center is shown in figure 2(a), symbol $|0\rangle$ and $|1\rangle$ represents the electron spin state number, where $|1\rangle$ state can be spin $m_s = -1$ or $m_s = +1$. We used -1 for our work because it is easier to control due to its lower transition energy compared to the $m_s = +1$ transition [5]. The symbol $|\downarrow\rangle$ and $|\uparrow\rangle$ are the states of the ^{13}C nuclear spin. In electron spin $|0\rangle$ manifold, the nuclear spin can oscillate between the states $|\downarrow\rangle$ and $|\uparrow\rangle$ with the Larmor precession frequency $\omega_L = 2\pi/\tau_L$. In electron spin $|1\rangle$ manifold, the hyperfine interaction introduces an energy shift between state $|\downarrow\rangle$ and $|\uparrow\rangle$ amounting to a frequency ω_1. From the diagram, if we weakly drive the electronic spin state transition $|0\rangle|\downarrow\rangle \leftrightarrow |1\rangle|\downarrow\rangle$ (blue transition), with the Rabi frequency $\Omega_{\text{weak}} < \omega_1$, only population of the $|0\rangle|\downarrow\rangle$ will be excited to electron spin $|1\rangle|\downarrow\rangle$ manifold. In contrast, if we drive the system with a strong microwave pulse, with Rabi frequency $\Omega_{\text{strong}} > \omega_1$, the whole population of the electron spin will be excited from electron spin $|0\rangle$ to electron spin $|1\rangle$ (red transitions).

To characterize the system, we performed pulsed optically detected magnetic resonance (pulsed-ODMR) experiment. We used the microwave with a pulse width of 1120 ns and a power of –14.4 dBm for pulsed-ODMR experiment to avoid a power broadening effect [15]. At a magnetic field $B_z = 46$ G, figure 2(b) shows 4 transitions at frequencies of 2.7399, 2.7429, 2.7464 and 2.7494 GHz, respectively. These 4 transitions include the effect of $\omega_1 = 2\pi \times 6.5$ MHz hyperfine splitting from the ^{13}C nuclear spin and ~3 MHz hyperfine splitting from ^{15}N. We average the 4 frequencies from the fitting to obtain the center frequency of 2.7446 GHz as the strong transition frequency between state $|0\rangle$ and $|1\rangle$ to use as a frequency for the strong transition, which power is set to +13.3 dBm to obtain the microwave π pulse duration of 30 ns. In addition, we chose the center of two dips from the left as a weak resonance transition frequency between $|0\rangle|\downarrow\rangle$ and $|1\rangle|\downarrow\rangle$, which is 2.7414 GHz, which power is set to +1.3 dBm to obtain the microwave π pulse duration of 120 ns. Figure 2(c) shows the experimental data from driving the resonance of the

weak (blue) and strong (red) transitions, these two have Rabi frequencies of $\Omega_{\text{weak}} = 2\pi \times 4.59$ MHz and $\Omega_{\text{strong}} = 2\pi \times 17.86$ MHz from the fitting, respectively. The contrast between two datasets is about of ½ corresponding with driving full and half of the population in the electron spin $|0\rangle$ manifold.

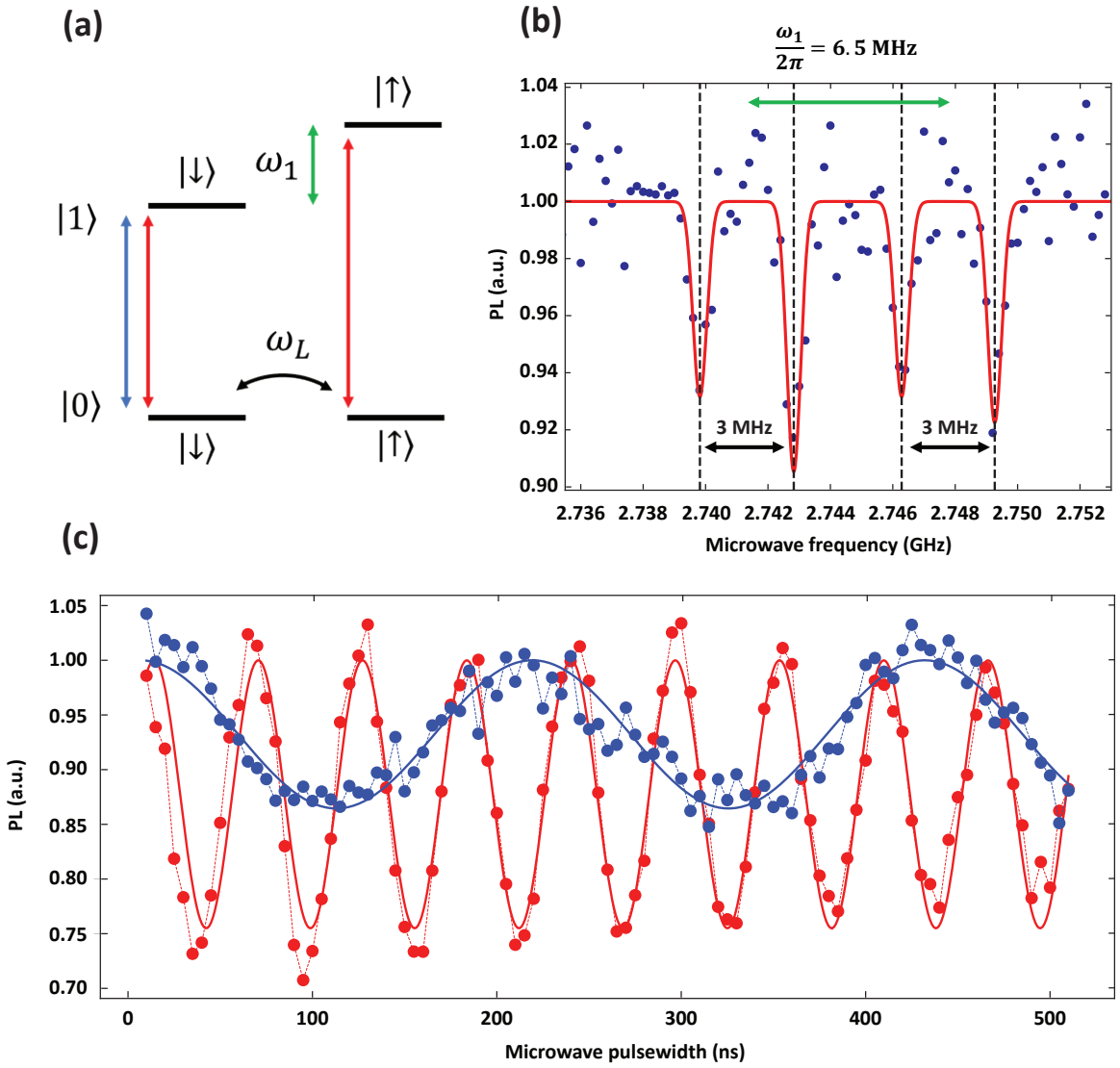

Figure 2. (a) The energy diagram for the coupled NV center electron spin and nuclear spin of the ^{13}C. The symbols $|0\rangle$ and $|1\rangle$ represent the electron spin state number, while $|\downarrow\rangle$ and $|\uparrow\rangle$ denote spin up and spin down of the nuclear spin. The strong microwaves can drive both transitions (red lines) of the nuclear spin; in contrast, the weak microwaves can drive only on transition (blue line) as shown in the diagram. (b) The pulsed-ODMR result at magnetic field $B_z = 46$ G. (c) The electron Rabi oscillation data obtained by driving the resonance frequencies of the weak (blue) and strong (red) transitions with Rabi frequencies of $\Omega_{\text{weak}} = 2\pi \times 4.59$ MHz and $\Omega_{\text{strong}} = 2\pi \times 17.86$ MHz, respectively.

3.2 Nuclear spin free precession

The microwave pulse sequence for observing the nuclear spin free precession is shown in figure 3(a). At first, assume that the initial state after initialization with the green laser is in a coupled NV center electron spin$|0\rangle$ and the ^{13}C nuclear spin in form $\alpha|\downarrow\rangle + \beta|\uparrow\rangle$, $|\psi\rangle = |0\rangle\otimes(\alpha|\downarrow\rangle + \beta|\uparrow\rangle)$. To prepare the pure state in $|0\rangle|\downarrow\rangle$, we started by applying a weak π pulse to selectively excite the entire population of spin $|\downarrow\rangle$ into electron spin $|1\rangle$ manifold, leaving electron spin $|0\rangle$ manifold only with the spin $|\uparrow\rangle$ population. After waiting for time $\frac{\tau_L}{2}$, the spin state $|0\rangle|\uparrow\rangle$ oscillates into $|0\rangle|\downarrow\rangle$, leaving the system in only spin $|\downarrow\rangle$ with the electron spin in both $|0\rangle$ and spin $|1\rangle$ manifolds, changing the total state to $\alpha|1\rangle|\downarrow\rangle + \beta|0\rangle|\downarrow\rangle$. Then, we used the green laser with a pulse width of 130 ns to repolarize the electron spin into spin $|0\rangle$ to obtain the total state in form $|0\rangle|\downarrow\rangle$. In the free precession duration, the nuclear spin precesses with the Larmor period $\tau_L = 2\pi/\omega_L$, then the weak π pulse was used again to map the nuclear spin population back onto the electron spin state, creating an oscillation.

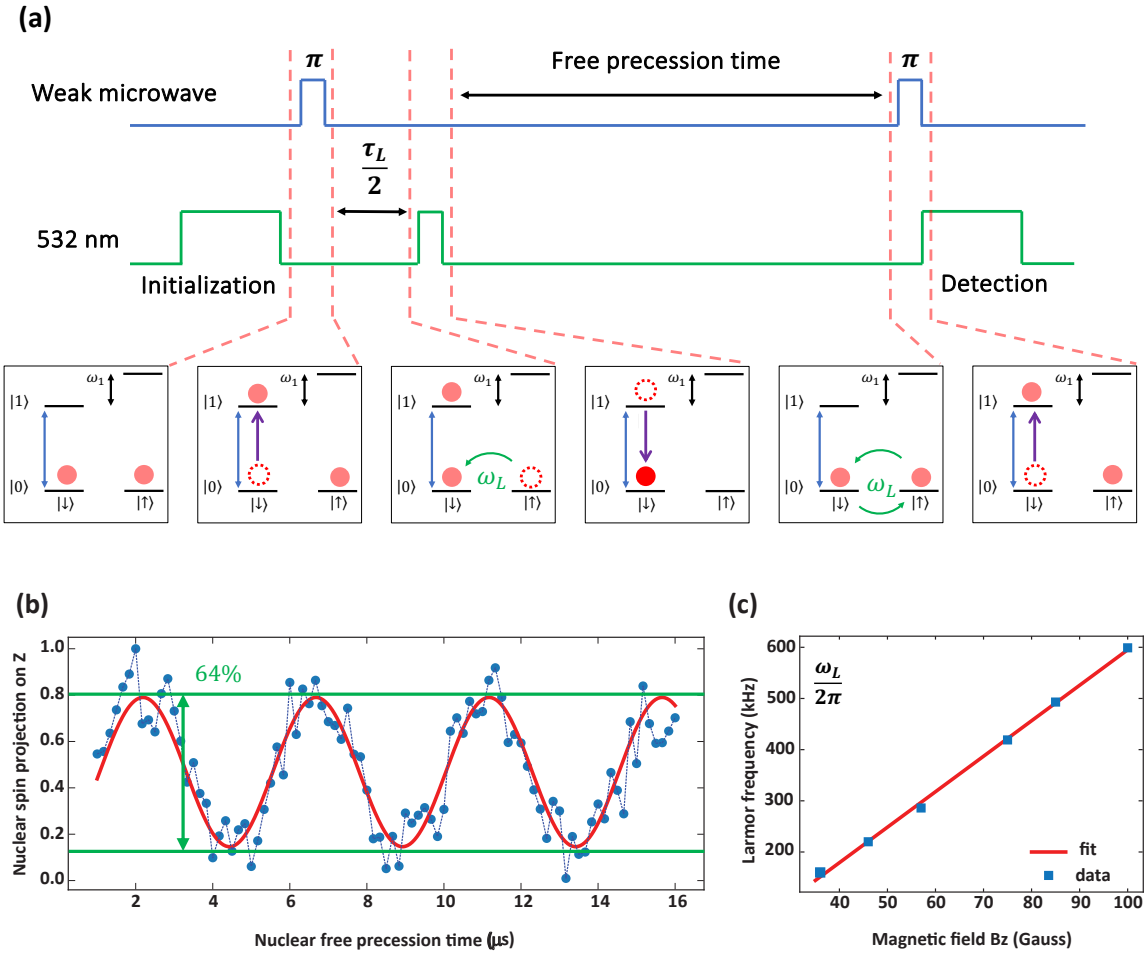

Figure 3. (a) Diagram representation spin state evolution during the nuclear free precession operation. The red circles represent the state population and green arrow show the changing of state and the blue arrow represent electron weak transition. (b) Nuclear free precession graph in a magnetic field $B_z = 46$ G. The blue dot represents experimental data, and the red line indicates the curve fitting. Nuclear spin flip from state $|\downarrow\rangle$ to $|\uparrow\rangle$ in every $\tau_L = 4.49$ μs. (c) The Larmor precession curve of the single nuclear spin with an enhanced gyromagnetic ratio $\gamma_{\text{eff}} = 6.9 \pm 0.1$ kHz/G.

Figure 3(b) shows the nuclear spin precession data at external magnetic field $B_z = 46$ G with the Larmor period $\tau_L \approx 4.49$ μs and the contrast of ~64%. The peaks and dips in the signal correspond to the spin $|\uparrow\rangle$ and spin $|\downarrow\rangle$, respectively. After that, we varied the magnitude of the magnetic field and observed the expected linear relationship between the Larmor frequency and the magnetic field, as shown in figure 3(c). Due to the coupling between the electron and the nuclear spin, the electron spin introduces an additional magnetic field effect on the nuclear spin, which results in an increase in the nuclear spin's gyromagnetic ratio [5, 16, 17]. We fit the data with a linear equation $\frac{\omega_L}{2\pi} = \gamma_{eff} B + \frac{\omega_0}{2\pi}$, and obtained an enhanced gyromagnetic $\gamma_{eff} = 6.9 \pm 0.1$ kHz/G. This value is significantly higher than the bare gyromagnetic ratio of ^{13}C ($\gamma_c = 1.07$ kHz/G), and has an offset due to the hyperfine interactions with the electronic spin of the NV center.

3.3 Nuclear spin phase accumulation

The hyperfine interaction affects nuclear spin of ^{13}C let the spin up in electron spin $|1\rangle$ manifold, making the spin $|\uparrow\rangle$ and spin $|\downarrow\rangle$ energies differ by a frequency ω_1, which can be stored in term of phase information of the NV. We performed the experiment followed from the pulse diagram in figure 4(a) to observe this effect. In this process, the second microwave source is used for driving electron in both transitions with strong π pulse. After the state was initialized in $|0\rangle|\downarrow\rangle$, and then wait for time $\frac{\tau_L}{4}$ has elapsed, the nuclear spin precesses into the superposition state $\frac{1}{\sqrt{2}}|0\rangle(|\downarrow\rangle + i|\uparrow\rangle)$. Next, we applied the strong π pulse to drive all population of the nuclear spin into electron spin $|1\rangle$ manifold, letting the spin state becomes $\frac{1}{\sqrt{2}}|1\rangle(|\downarrow\rangle + i|\uparrow\rangle)$. In the electron spin $|1\rangle$ manifold, the nuclear spin state $|\uparrow\rangle$ accumulate phase difference $\omega_1\tau$ with respect to the spin state $|\downarrow\rangle$ leaving the total state in $\frac{1}{\sqrt{2}}|1\rangle\left(|\downarrow\rangle + ie^{-i\omega_1}|\uparrow\rangle\right)$. The strong π pulse was used again to map the state back onto the electron spin $|0\rangle$ manifold and then, waiting another $\frac{\tau_L}{4}$, we can obtain the state in form $\frac{1}{2}|0\rangle\left((1 - e^{i\omega_1\tau})|\downarrow\rangle + i(1 + e^{i\omega_1\tau})|\uparrow\rangle\right)$ The final state can be read out optically and the probability of the nuclear spin up ($P_\uparrow$) and spin down ($P_\downarrow$) are given by

$$P_\uparrow = \frac{1}{2}(1 + \cos(\omega_1\tau)) \tag{2}$$

$$P_\downarrow = \frac{1}{2}(1 - \cos(\omega_1\tau)) \tag{3}$$

For an ideal system, the data should have an oscillation as depicted in figure 4(b), which is obtained from Eq. (2). The experimental data in figure 4(c) has a precession frequency of 6.5 MHz that correspond to $\omega_1 = 2\pi \times 6.5$ MHz hyperfine splitting. From this process, the signal should have the nuclear spin population close to the nuclear precession data, as we already prepared the state follow from the diagram in figure 3(a) before performing the nuclear spin phase accumulation experiment. However, we observed some population loss from the experiment, indicated by the reduction in contrast compared to the result in figure 3(b) (the contrast of the signal is only about of 37%). The result of the population loss can be noticed especially when the experiment is performed over 15 μs, as shown in figure 4(d), where the precession exhibits two beating oscillations. Fourier transformation reveals two frequencies at 0.215 MHz and 6.5 MHz, corresponding to the Larmor frequency of the ^{13}C nuclear spin and hyperfine splitting frequency, as shown in the inset. This proof that during the nuclear spin phase

accumulation experiment, there remains some nuclear spin population that was not excited by the strong π pulse in the electron spin $|0\rangle$ manifold.

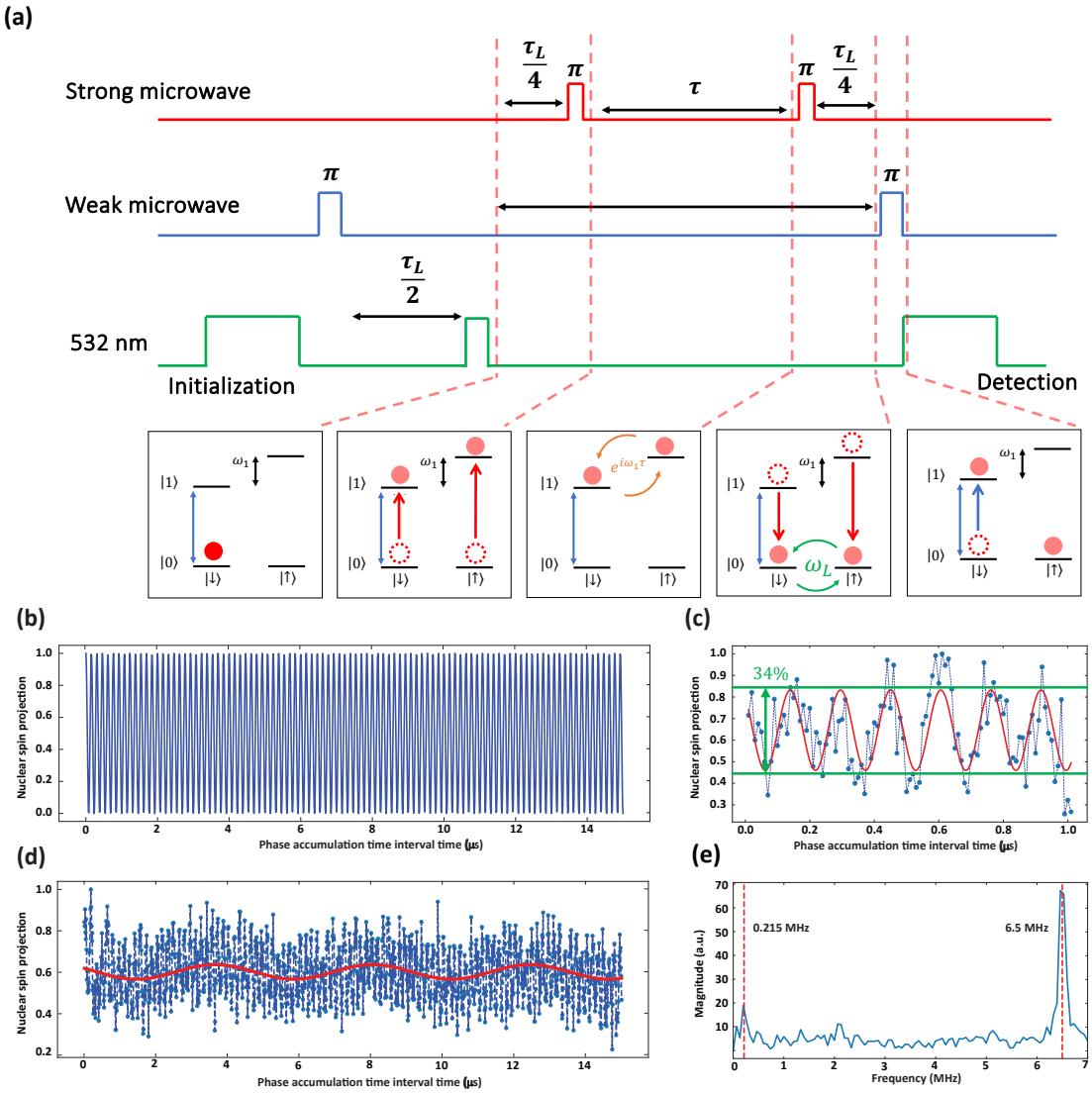

Figure 4. (a) The pulse experiment diagram for observing the phase accumulation of the nuclear spin. (b) The ideal nuclear spin projection out to 15 μs. (c) Nuclear spin projection shows oscillation with frequency $2\pi \times 6.5$ MHz (d) The ^{13}C nuclear spin phase accumulation out to 15 μs shows two oscillations in the data. The dash line show oscillation effect from hyperfine interaction and the red line shows oscillation match with the Larmor frequency. (e) Fourier transform of the data in (d). The result shows the peaks at 0.215 MHz and 6.5 MHz.

4. Conclusion

We demonstrated characterization and control of a ^{13}C nuclear spin information by utilizing only MW signal control. By only manipulating the electron spin, we were able to extract the free precession data of the nuclear spin. Furthermore, by varying the external magnetic field, we could observe the enhanced gyromagnetic ratio of the ^{13}C nuclear spin from the hyperfine effects, which

is ~ 4.06 enhanced from the bare ^{13}C nuclear spin. Additionally, we performed a nuclear spin phase accumulation measurement in the electronic spin-1 manifold, enabling the observation of hyperfine interaction stored in terms of phase information between nuclear spin superposition. Furthermore, an unexpected population loss during the nuclear phase accumulation experiment in figure 4(c) was observed, resulting in reduced contrast compared to the nuclear spin free precession data in figure 3(b) (from 64% to 37%). Fourier transformation analysis revealed two distinct frequencies corresponding to the Larmor of the ^{13}C nuclear spin and the hyperfine splitting frequency. These findings suggest incomplete population transfer and the presence of a non-perfectly polarized state in our system. Some populations of the nuclear spin remain in electron spin $|0\rangle$ manifold during the operation. This phenomenon may arise from several sources, including the fact that the strong π pulse is still insufficient (low microwave intensity) to drive the entire population from electron spin $m_s = 0$ to $m_s = -1$ and the resonance frequency for the strong π pulse might not perfectly match the transition frequency because our system contains the ^{15}N in mixed spin state. Understanding and addressing these effects are crucial for accurate interpretation of our data and for the advancement of our research. This will enable us to refine our experimental procedures and optimize our system to obtain the high contrast after manipulating the nuclear spin by using the strong microwave for future studies.

Acknowledgments

This research has received funding support from the NSRF via the Program Management Unit for Human Resources & Institutional Development, Research and Innovation [grant number B39G670018]. Kritsana Saego has received financial support from the Development Promotion of Science and Technology (DPST) scholarship.

References

[1] Pezzagna S and Meijer J 2021 *Appl. Phys. Rev.* **8** 011308
[2] Suter D and Jelezko F 2017 *Progress in Nuclear Magnetic Resonance Spectroscopy* **98** 50–62
[3] Barry J F, Jennifer M S, Erik B, Matthew J T, Connor A H, Linh M P and Ronald L W 2020 *RMP* **92** 015004
[4] Gruber A, Drabenstedt A, Tietz C, Ludovic F, Wrachtrup J and Borczyskowski C 1997 *Science* **276** 2012
[5] Childress L, Gurudev Dutt M V, Taylor J M, Zibrov A S, Jelezko F, Wrachtrup J, Hemmer P R, and Lukin M D 2006 *Science* **314** 281–85
[6] Jelezko F, Gaebel T, Popa I, Domhan M, Gruber A and Wrachtrup J 2004 *Phys. Rev. Lett.* **93** 130501
[7] Smeltzer B, McIntyre J and Childress L 2009 *Phys. Rev. A* **80** 050302
[8] Zhang J, Swathi S H and Suter D 2019 *Phys. Rev. Appl.* **12** 064047
[9] Gurudev Dutt M V, L Childress, L Jiang, E Togan, J Maze, F Jelezko, A S Zibrov, P R Hemmer and Lukin M D 2007 *Science* **316** 1312–16
[10] Kagami S, Shikano Y, and Asahi K 2011 *Physica E* **43** 761–65
[11] Sangtawesin S, Dwyer B L, Srinivasan S, Allred J J, Rodgers L V, De Greve K, Stacey A, Dontschuk N, O'Donnell K M, Hu D and Evans D A 2019 *Phys. Rev. X* **9** 031052
[12] Manson N B, Harrison J P and Sellars M J 2006 *Phys. Rev. B* **74** 104303
[13] Gupta A, Hacquebard L and Childress L 2016 *JOSA B* **33(3)** 28–34
[14] Smeltzer B, Childress L and Gali A 2011 *New Journal of Physics* **13** 025021
[15] Dréau A, Lesik M, Rondin L, Spinicelli P, Arcizet O, Roch J F and Jacques V 2011 *Phys. Rev. B* **84** 195204
[16] Chen M, Hirose M and Cappellaro P 2015 *Phys. Rev. B* **92** 020101
[17] Sangtawesin S, McLellan, Myers C A, Jayich B A, Awschalom D D and Petta J R 2016 *New Journal of Physics* **18** 083016